Forward and retrograde precession from the ECE2 Lagrangian

M. W. Evans*, H. Eckardt†
Civil List, A.I.A.S. and UPITEC

(www.webarchive.org.uk, www.aias.us,
www.atomicprecision.com, www.upitec.org)

3 Discussion of numerical results and graphics

3.1 Four theories of relativistic motion

We give some refinement of the equations for forward and retrograde precession. First we present the equations of four formulations of the relativistic equations of motion derived from the relativistic Lagrangian (1).

3.1.1 Relativistic Lagrangian model with t

With the Lagrange variables X and Y the following equations of motion are obtained from the Euler-Lagrange equations (5,6):

$$\ddot{X} = MG\,\frac{\dot{X}Y\,\dot{Y} + X\,\dot{X}^2}{\gamma c^2\left(Y^2+X^2\right)^{3/2}} - \frac{MGX}{\gamma(X^2+Y^2)^{3/2}}, \tag{60}$$

$$\ddot{Y} = MG\,\frac{\dot{Y}X\,\dot{X} + Y\,\dot{Y}^2}{\gamma c^2\left(X^2+Y^2\right)^{3/2}} - \frac{MGY}{\gamma(X^2+Y^2)^{3/2}}. \tag{61}$$

These can be combined in vector form as

$$\ddot{\mathbf{r}} = \frac{M\,G}{\gamma\,r^3}\left(\frac{\dot{\mathbf{r}}\,(\dot{\mathbf{r}}\cdot\mathbf{r})}{c^2} - \mathbf{r}\right) \tag{62}$$

with

$$r = \left(X^2+Y^2\right)^{1/2}. \tag{63}$$

*email: emyrone@aol.com
†email: mail@horst-eckardt.de

3.1.2 Relativistic Lagrangian model with τ

In standard relativistic Lagrange theory the time derivative in the Euler-Lagrange equations (5-6) is defined by the proper time τ:

$$\frac{\partial \mathscr{L}}{\partial X} = \frac{d}{d\tau}\frac{\partial \mathscr{L}}{\partial \dot{X}}, \tag{64}$$

$$\frac{\partial \mathscr{L}}{\partial Y} = \frac{d}{d\tau}\frac{\partial \mathscr{L}}{\partial \dot{Y}}. \tag{65}$$

This leads to an additional factor of $1/\gamma$ in Eqs. (60, 61):

$$\ddot{X} = MG\,\frac{\dot{X}Y\,\dot{Y} + X\,\dot{X}^2}{\gamma^2 c^2\left(Y^2+X^2\right)^{3/2}} - \frac{MGX}{\gamma^2(X^2+Y^2)^{3/2}}, \tag{66}$$

$$\ddot{Y} = MG\,\frac{\dot{Y}X\,\dot{X} + Y\,\dot{Y}^2}{\gamma^2 c^2\left(X^2+Y^2\right)^{3/2}} - \frac{MGY}{\gamma^2(X^2+Y^2)^{3/2}}, \tag{67}$$

and in vector form:

$$\ddot{\mathbf{r}} = \frac{M\,G}{\gamma^2\,r^3}\left(\frac{\dot{\mathbf{r}}\,(\dot{\mathbf{r}}\cdot\mathbf{r})}{c^2} - \mathbf{r}\right). \tag{68}$$

3.1.3 Relativistic Newton equation

The relativistic Newton equation (21, 22), as derived in section 2 from the vector form (18) of the Euler Lagrange equations, is:

$$\ddot{\mathbf{r}} = -\frac{M\,G}{\gamma^3\,r^3}\,\mathbf{r}. \tag{69}$$

Here a factor of γ^3 appears in the denominator, and there is no additional velocity dependence as in (62) and (68).

3.1.4 Minkowski force

The Minkowski force equations can be derived from Minkowski theory directly and contains one more γ factor in the denominator:

$$\ddot{\mathbf{r}} = -\frac{M\,G}{\gamma^4\,r^3}\,\mathbf{r}. \tag{70}$$

3.1.5 Comparison of equations

All four equations have been solved numerically for the S2 star as described in UFT 375 in detail. Our first focus is on the angular momentum. In both Lagrange theories (62) and (68) the relativistic angular momentum is conserved by construction (Figs. 1 and 2). For the relativistic Newton and Minkowski force only the non-relativistic angular momentum is conserved (Figs. 3 and 4), giving an inconsistent result. There is no simple explanation available since the relativistic angular momentum was used in Eq. (14).

Precession is negative (or retrograde) for both the Minkowski and relativistic Newton force. From Lagrange theory equations the precession is positive.

	T [yr]	$r_{\max}$ [10^{14} m]	ϵ	$\Delta\phi$ [rad]	const. of motion
Euler-Lagr. t	15.50	2.78609	0.88712	$5.9033{\cdot}10^{-4}$	$L_{\rm rel}$
Euler-Lagr. τ	15.57	2.79440	0.88746	$7.5090{\cdot}10^{-7}$	$L_{\rm rel}$
Rel. Newton	15.50	2.78621	0.88720	$-1.7697{\cdot}10^{-3}$	$L_{\rm non-rel}$
Minkowski	15.06	2.79452	0.88753	$-2.3585{\cdot}10^{-3}$	$L_{\rm non-rel}$
Experiment	15.56	2.68398	0.8831	-0.017... +0.035	

Table 1: Parameters of S2 star orbit ($v_0 = 7.7529648 \cdot 10^6$ m/s, various calculations and experiment).

However precession is extremely small in the τ version of Lagrangian theory. It is barely above the numerical precision limit of 10^{-8} rad as determined in UFT 375. There is also a logical problem for the Lagrange theory based on proper time τ. All quantities are computed in the observer frame but the time derivative of $\partial L/\partial\dot{r}$ is computed for the frame local to the orbiting mass. This seems to be inconsistent. Therefore the Lagrange theory based on observer time t seems to be the best choice for a consistent overall description of relativistic effects. A comparison of all four theory variants is made in Table 1 for the orbit of the S2 star. The differences in maximum radius and eccentricity are marginal.

3.2 Spin connection vector

The spin connection vector $\boldsymbol{\kappa}$ can be computed from the solution of orbit trajectories in several degrees of approximation. By Eq. (52) we have one equation for both components κ_X and κ_Y. Under the assumption that the κ's vary only slowly with time, we can take the time derivative of this equation as a second equation, obtaining

$$\kappa_X X + \kappa_Y Y = -1, \tag{71}$$

$$\kappa_X \dot{X} + \kappa_Y \dot{Y} = 0. \tag{72}$$

Solving these equation set, we obtain

$$\kappa_X = \frac{\dot{Y}}{\dot{X}\,Y - X\,\dot{Y}}, \tag{73}$$

$$\kappa_Y = -\frac{\dot{X}}{\dot{X}\,Y - X\,\dot{Y}}. \tag{74}$$

We see that the κ's nevertheless depend on time since this is the case for the trajectories $X(t)$, $Y(t)$ and their derivatives. These trajectories are graphed in Figs. 5 and 6 for the S2 star. Due to the high ellipticity of the orbit, there are sharp peaks at periastron. The approximate solution (73, 74) is graphed in Fig. 7. There is high similarity to the derivatives $\dot{X}$, $\dot{Y}$ of Fig. 6, with interchange of X and Y and the sign of one component.

Eq. (52) was derived from the Coulomb-like field equation (50). Instead of taking an additional time derivative, we can use the static Ampere law (51). In

two dimensions there is only a Z component of the curl operator, giving in total the equation set

$$\kappa_X X + \kappa_Y Y = -1, \tag{75}$$
$$\kappa_X Y - \kappa_Y X = 0. \tag{76}$$

This can be solved by computer algebra directly:

$$\kappa_X = -\frac{X}{X^2 + Y^2}, \tag{77}$$
$$\kappa_Y = -\frac{Y}{X^2 + Y^2}. \tag{78}$$

The denominator is always positive now, leading to a smoother curve of the κ's except at periastron, see Fig. 8. This fact should give further serious concern for Einsteinian general relativity where infinities ("black holes") are built in by construction. As we can see from these examples, in nature there are no infinities, and improving the descriptional approach removes infinities. This stage has never been reached by the Einsteinian theory.

Instead of solving the field equations (75, 76) for κ, we can alternatively solve them for X, Y. This leads to

$$X = -\frac{\kappa_X}{{\kappa_X}^2 + {\kappa_Y}^2}, \tag{79}$$
$$Y = -\frac{\kappa_Y}{{\kappa_X}^2 + {\kappa_Y}^2}. \tag{80}$$

Obviously the orbit is entirely determined by the spin connection, a completely new result of relativistic gravitational physics. Spin connections and orbit coordinates are mutually symmetric, showing some sort of symmetry, which perhaps can be interpreted as a correspondence between configuration and momentum space.

This offers the capability of investigating what happens when the spin connections are slightly modified, a kind of spacetime or aether engineering. As an example we modify the Y component of the spin connection vector by

$$\kappa_Y \to \kappa_Y - t \cdot 10^{-17}. \tag{81}$$

The Y component is continuously decreased. The result is a retrograde precession of the orbit as shown in Fig. 9. So any kind of precession can - besides other methods - be evoked by aether engineering.

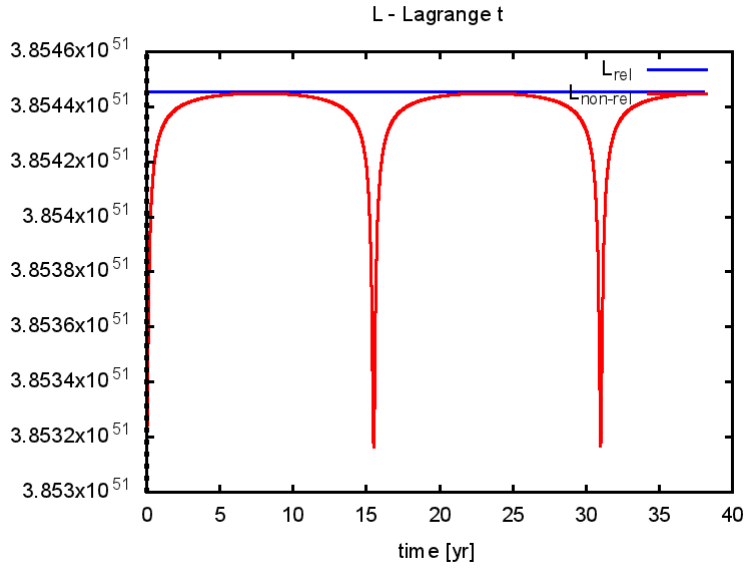

Figure 1: Angular momentum, Euler-Lagrange equations with t.

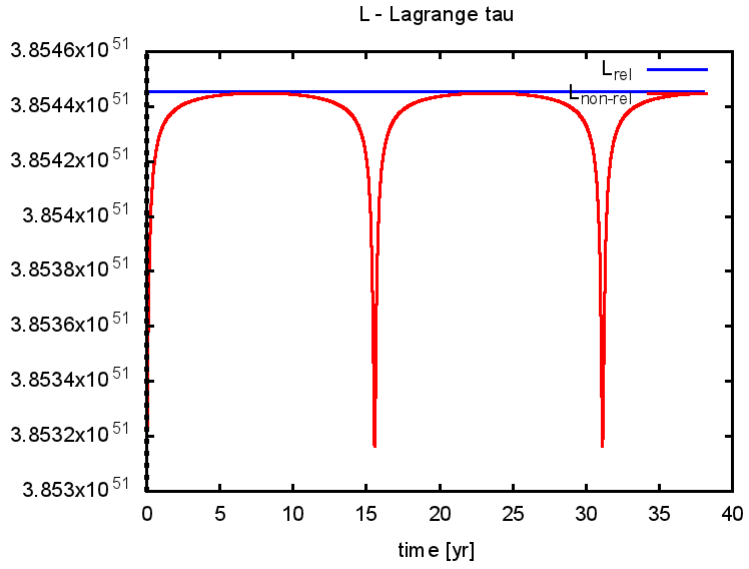

Figure 2: Angular momentum, Euler-Lagrange equations with τ.

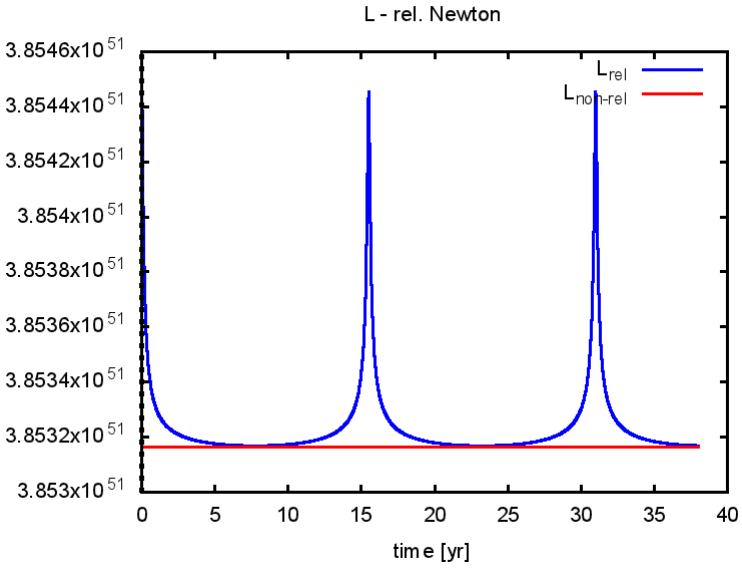

Figure 3: Angular momentum, relativistic Newton Equation.

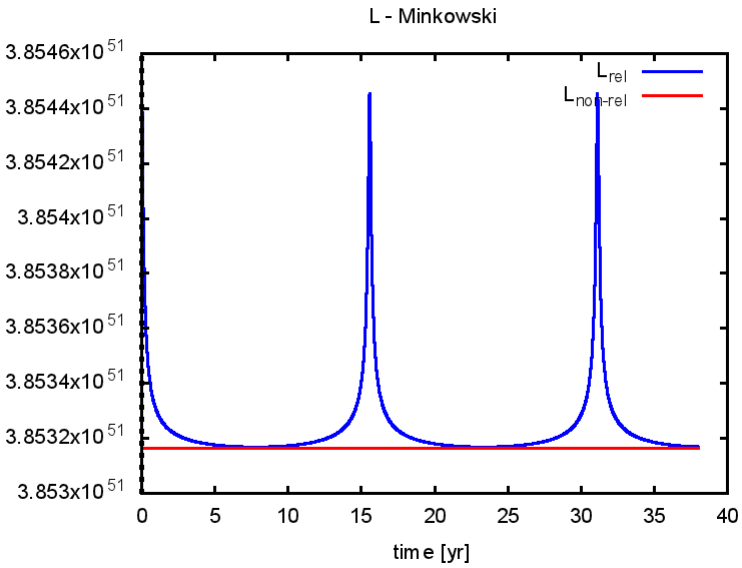

Figure 4: Angular momentum, Minkowski Equation.

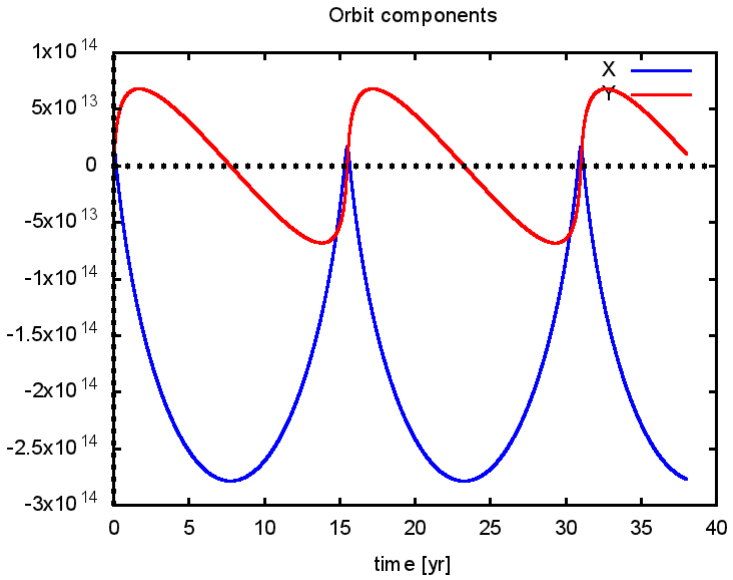

Figure 5: Orbital trajectories for S2 motion.

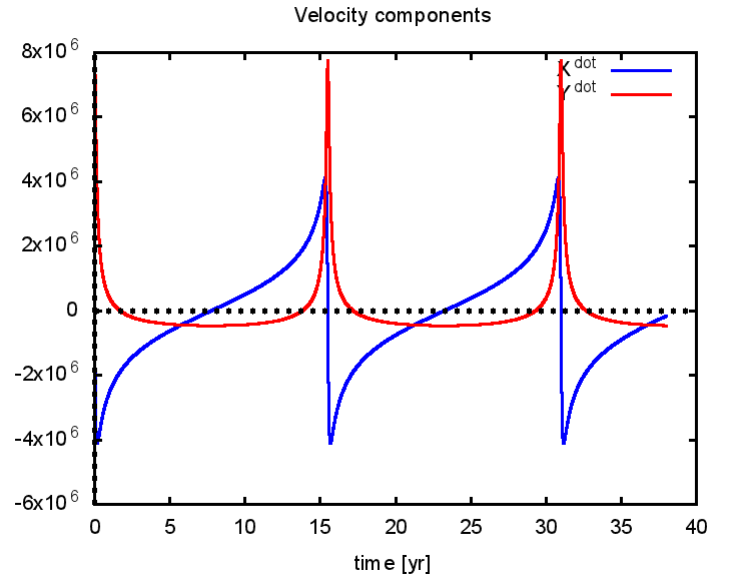

Figure 6: Orbital time derivative trajectories for S2 motion.

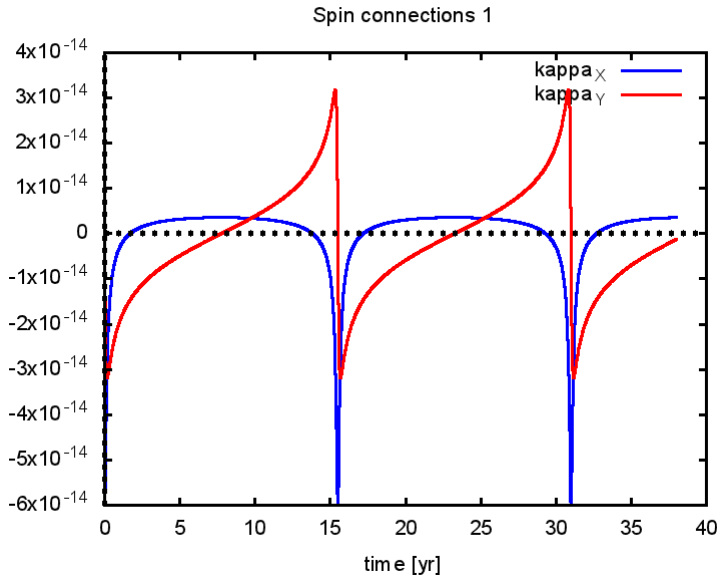

Figure 7: Spin connection components for approximation (73, 74).

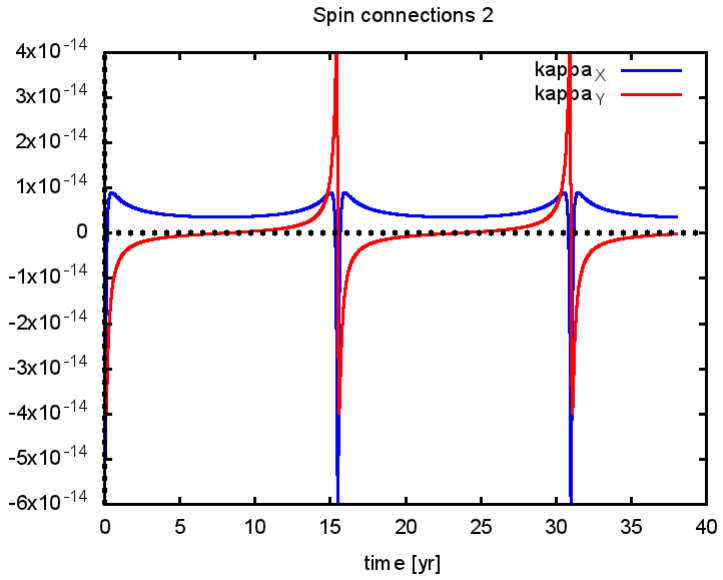

Figure 8: Spin connection components for exact solution (77, 78).

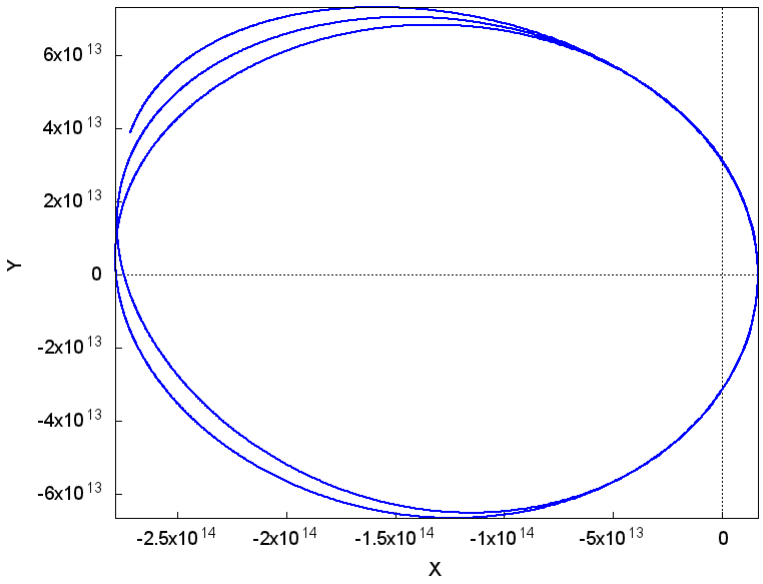

Figure 9: Retrograde precessing orbit evoked by aether engineering (modified spin connection).